Physical Review E, Volume 81, Issue 6, 2010, 061503 [5 pages]

# Boundary slip dependency on surface stiffness

Nikolaos Asproulis and Dimitris Drikakis*

*Fluid Mechanics & Computational Science Group,*

*Department of Aerospace Sciences,*

*Cranfield University, United Kingdom*

(Dated: March 26, 2010)

## Abstract

Nanofluidics is an emerging and rapidly growing field that provides fertile ground for developing innovative strategies and novel devices for a number of disciplines including medicine, biology, and engineering. Here we draw attention to the implications of surface stiffness on the slip process aiming to obtain a better insight of the momentum transfer at nano scales. The surface stiffness is modelled through the stiffness $\kappa$ of spring potentials that are employed for constructing the thermal walls. It is shown that variations of stiffness $\kappa$ influence the slip mechanism either towards slip or stick conditions. Increasing the values of $\kappa$ alters the oscillation frequency and the mean displacement of the wall particles towards higher and lower values respectively. Our results suggest that the amount of slip produced as a function of stiffness follows a common pattern that is modelled through a fifth order polynomial function.

PACS numbers: 68.08.-p, 83.10.Rs, 83.50.Lh, 83.50.Rp, 68.35.Ct, 47.61.-k

*Electronic address: d.drikakis@cranfield.ac.uk

## I. INTRODUCTION

Over the past decade micro and nanofluidics have emerged as vital tools in the ongoing drive towards the development of nano-scale analysis and manufacturing systems. As the devices' operational dimensions are downsized to micro and nano scales the surface-to-volume ratio increases and the interfacial interactions dominate the flow phenomena. The surface interactions effects are macroscopically formulated via appropriate boundary conditions. In the majority of the macroscale flows the fluid is considered to be immobile near the solid boundary; however as the scales shrink a number of experimental studies [1–3] revealed the presence of slippage. In these cases, where the continuum no-slip approximation breaks down, the slip's magnitude is quantified through a parameter named as slip length ($L_s = \frac{u_{slip}}{\partial u/\partial n}$), which represents the extrapolated distance from the wall to the point with zero tangential velocity component. Surface structure, wettability and, nanoscale roughness are some of the factors that have been recognised to affect slippage phenomena [4, 5]. Generally, the parameters that contribute to slip generation along with their implications to the slip's magnitude are not explicitly known and fully understood [6]. Therefore, identifying and quantifying their impact poses a great challenge that will assist the development of micro and nanofluidic devices.

High fidelity computational modelling has been embraced to compliment experiments related to slippage effects, primarily due to accuracy and precision difficulties involved in measuring physical quantities at nano scales. Specifically, molecular dynamics [7–10] (MD) simulations, have been employed to study the slip's mechanism and enlighten the impact of parameters such as nanoroughness or surface wettability to the slip's magnitude.

It is commonly recognised [6] that surface corrugation can greatly influence the interfacial flow characteristics. However, it is still unclear whether it contributes towards slip or stick conditions, since experimental evidence [3, 11, 12] suggests that both possibilities exist. Numerically, although a number of studies [13, 14] have been performed, the slip's decreased or increased rate as a factor of roughness, has not been fully quantified. An important component for the slip process, that may elucidate the variability of the experimental and numerical outcomes, is surface stiffness. In the current study MD simulations are employed to study the slip length's dependency on the wall stiffness for a Lennard-Jones (LJ) fluid.

## II. SIMULATION METHOD

The computational domain considered for the current numerical experiments consists of monoatomic fluid particles confined by two stationary thermal walls separated by distance $L_y$ along the $y$ direction. The size of the computational domain is $L_x = 16.97\sigma$, $L_y = 34.64\sigma$ and $L_z = 6.53\sigma$, where $\sigma$ is the molecular length scale; and periodic boundary conditions are applied in the parallel to the walls directions $x$ and $z$. The interatomic interactions among the fluid molecules are modelled through a LJ potential which for a pair of molecules $i, j$ with distance $r_{ij}$ is

$$\nu_{ij}^{LJ}(r_{ij}) = 4\epsilon \left[(\sigma/r_{ij})^{12} - (\sigma/r_{ij})^{6}\right] \tag{1}$$

where $\epsilon$ is the characteristic energy level. All the interatomic interactions are truncated at a cut-off distance $r_c = 2.2\sigma$. The fluid's density is selected to be $\rho_{fluid} = 0.81\ m\sigma^{-3}$, where $m$ is the mass of a fluid's molecule, and corresponds to the generation of 2880 particles. A constant external force $f_x$, along the $x$ direction, is applied to each fluid molecule to drive the flow. The simulations have been performed for a range of force's values spanning from $f_x = 0.005\ \epsilon\sigma^{-1}$ to $f_x = 0.015\ \epsilon\sigma^{-1}$ with step $0.0025\ \epsilon\sigma^{-1}$. The velocity profile from a continuum hydrodynamics perspective, assuming a slip velocity $u_{slip}$ at the solid boundary, is

$$u_x(y) = 0.5\mu^{-1}\rho f_x \left[(L_y/2)^2 - y^2\right] + u_{slip} \tag{2}$$

The parabolic velocity profile, described by Eq. 2, implies that the shear rate is proportional to the applied force and consequently force's variations corresponds to subsequent adjustments of the shear rate. Previous computational studies [7, 9, 15] have indicated a non linear relationship between the shear rate and the slip length. Therefore, aiming to minimise the shear rate's influences to the outcome's variability, the impact of the wall stiffness to the slip phenomena is studied for a broad range of shear rates. The magnitude of the applied force should be cautiously selected, since high force values can drive the system out of the linear response regime [16]. The excessive viscous heating of the system is dissipated through a Langevin thermostat [7], applied only in the $z$ direction to circumvent any possible influences to the flow direction. The equations of motion along the $z$ direction are

$$m\ddot{z}_i + m\Gamma\dot{z}_i = -\sum_{i\neq j} \frac{\partial V_{ij}}{\partial z_i} + \eta_i \tag{3}$$

where $\eta_i$ is a Gaussian distributed random force with zero mean $<\eta_i(t)>=0$ and variance $<\eta_i(0)\eta_j(t)>=2mk_BT\Gamma\delta(t)\delta_{ij}$, where $T=1.1\ \epsilon k_B^{-1}$ is the fluid's temperature. The friction coefficient has been selected to be $\Gamma=1.0\ \tau^{-1}$ throughout the simulations, aiming to minimise any undesirable effects to the self diffusion coefficient [9, 17]. The equations of motion are integrated through a velocity-Verlet algorithm [18] with time step $\delta t=0.001\tau$. A total number of $6\cdot10^5$ time steps have been performed for equilibration and afterwards another $6\cdot10^5$ for averaging.

Each of the solid walls is modelled as two (111) fcc lattice planes with density $\rho_{wall}=4.0\ m\sigma^{-3}$ corresponding to 528 particles with mass equal to the fluid ones. The wall particles interact with the fluid through a LJ potential with energy and length scales $\epsilon_{wf}$ and $\sigma_{wf}$ respectively. Generally, slippage phenomena are sensitive to the wall-fluid interactions and, particularly, as the wall's surface energy decreases, the amount of momentum transferred across the interface decreases leading to larger slip values [7]. Therefore, the effects of surface stiffness are studied for two sets of interfacial parameters (i) $\epsilon_{wf}=0.2\epsilon,\ \sigma_{wf}=0.75\sigma$ and (ii) $\epsilon_{wf}=0.4\epsilon,\ \sigma_{wf}=0.75\sigma$. Every wall particle $i$ is attached to its equilibrium lattice site $\boldsymbol{r}_0$ with an elastic spring force

$$\boldsymbol{F}=-\kappa\left(\boldsymbol{r}_i-\boldsymbol{r}_0\right) \tag{4}$$

where $\kappa$ is the wall's stiffness. Stiffness is a pivotal parameter that provides a link between the wall model and real materials and determines the wall's physical properties. Its values reveal the strength of particles' bonds and larger rates are related to higher melting points and Young's modulus. Their selection should not allow (i) the mean square displacement of the wall atoms to be larger than the Lidemann criterion of melting [9, 19] and (ii) the movement of the wall's atoms to be in a regime that cannot be entirely addressed in the molecular simulation's time step [9]. For the current study $\kappa$ ranges from $\kappa=100\ \epsilon\sigma^{-2}$ to $\kappa=1200\ \epsilon\sigma^{-2}$; this interval is consistent with typical $\kappa$ magnitudes employed in previous MD studies [9, 20, 21]. Although it is not straight forward to establish exact relations between simplified models, such as the one employed here for the wall, and real physical substances, the selected values of solid's stiffness corresponds to a broad range of real materials including silicon based structures, that are primarily used for microfluidic fabrications and typically their Young modulus is lower compared to the metals one [22]. The wall temperature is kept constant equal to $T_{wall}=1.1\ \epsilon k_B^{-1}$ during the simulations through a velocity rescaling thermostat [23].

In the employed model the walls' particles are allowed to vibrate around their crystalline sites based on a spring potential. Consequently, due to the absence of inter-atomic interactions, there is no solid elasticity in the wall and therefore, this model tends to neglect the molecular diffusion. Despite the absence of solid elasticity the thermal vibrations of the wall particles, that are frequently neglected in molecular studies [24, 25], are simulated effectively. Although this type of thermal walls is expected to provide slightly overestimated figures for the slip, due to the absence of solid elasticity, is widely adopted [24, 25] in the literature. In more sophisticated models, where the wall particles are not anchored to their lattice sites, the presence of inter-atomic interactions and molecular diffusion in the wall alters the original structure of the lattice and therefore, additional nanoscale roughness is introduced affecting the frictional coefficient. Outcomes from previous MD studies show small variations between models with and without solid elasticity [9, 26, 27].

## III. RESULTS AND DISCUSSION

Figure 1 shows examples of averaged fluid density profiles under different values of surface stiffness. These simulations have been carried out with interaction parameters $\epsilon_{wf} = 0.2\epsilon$, $\sigma_{wf} = 0.75\sigma$ and an external driving force $f_x = 0.0075\ \epsilon\sigma^{-1}$. A common element observed in the density distributions is their profound oscillations near the solid wall. Despite the changes in the surface stiffness, the density follows the same pattern, since the locations of its local maxima and minima remain almost constant, and rests to its bulk value after $(5-7)\ \sigma$. The variation of the spring stiffness primarily influences the density's absolute maximum value and for the simulations considered in Fig. 1 this value increases, with a non linear manner, as $\kappa$ increases from $\kappa = 100\ \epsilon\sigma^{-2}$ to $\kappa = 600\ \epsilon\sigma^{-2}$. Furthermore, deviations between the outcomes are reduced as higher surface stiffness rates are employed in the numerical simulations (see Fig. 1). Smaller $\kappa$ implies that the wall particles oscillate around their equilibrium positions with higher amplitude and lower frequency and therefore the fluid molecules can potentially travel closer to the solid wall [9]. As a consequence, a broader density profile is observed near the first peak. However, as the spring stiffness $\kappa$ increases its influence on the wall particles oscillations is primarily related to oscillation frequency rather than oscillation amplitude, which is mainly determined by the wall temperature [23]. Thus, its impact on the in-plane fluid's layering and hence on the density's profile is less apparent.

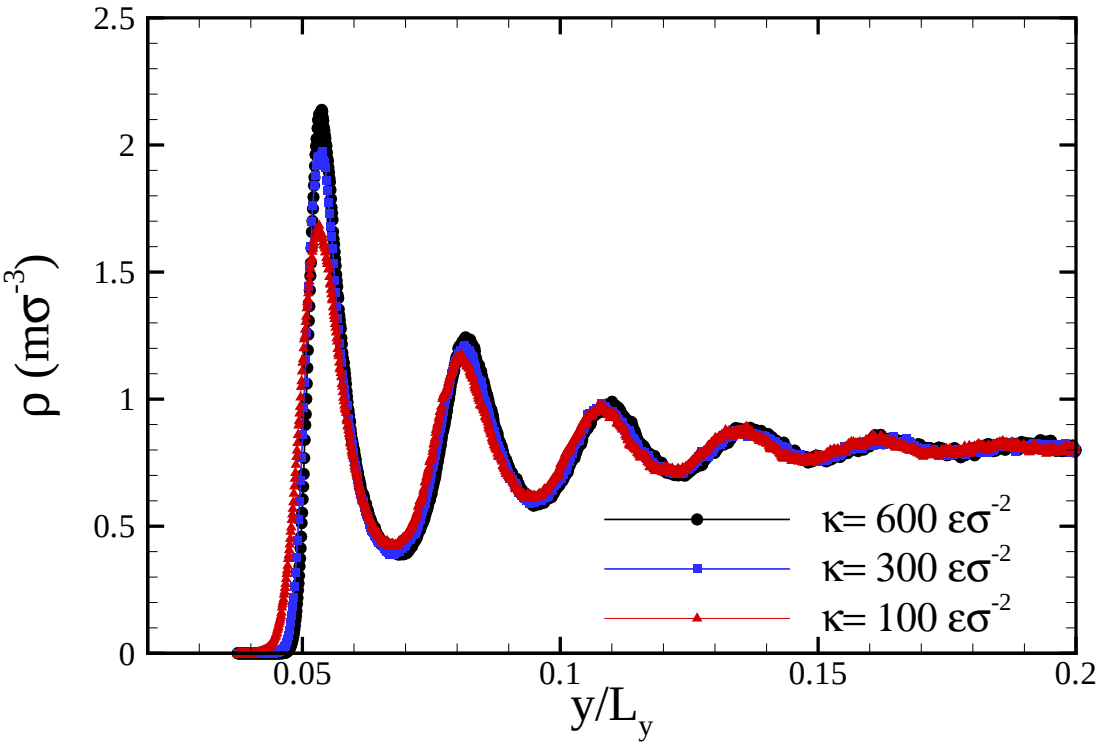


FIG. 1: Density profiles near the lower wall for various values of the spring stiffness $\kappa$ with $f_x = 0.0075\ \epsilon\sigma^{-1}$, $\epsilon_{wf} = 0.2\epsilon$.

Figure 2 shows the variation of the slip length for a certain value of stiffness $\kappa = 900\ \epsilon\sigma^{-2}$ as a function of the driving force $f_x$. Previous MD studies [7, 9] report that the slip length's variations are well described by a power law function

$$L_s(f_x) = L_s^0\ (1 - f_x/f_c)^{-0.5} \tag{5}$$

where $L_s^0$ represents a asymptotical value of the slip length as the shear rate tends to zero and $f_c$ corresponds a critical driving force value. As the driving force approaches this critical value $f_c$, the slip length appears to diverge[7]. In Fig. 2 the computational uncertainty in the slip length calculations is approximately 3%. The simulation data were fitted through Eq. 5 and the obtained parameters for $\epsilon_{wf} = 0.2\epsilon$ and $\epsilon_{wf} = 0.4\epsilon$ are $L_s^0 = 11.33\sigma,\ f_c = 0.0174\epsilon\sigma^{-1}$, and $L_s^0 = 6.88\sigma,\ f_c = 0.021\epsilon\sigma^{-1}$ respectively. In Fig. 2 it is noticed that the calculated slip lengths are in good agreement with analytical descriptions derived by previous studies [7, 9] and it is shown that the change rate of the slip length increases as the driving force moves towards to its critical value.

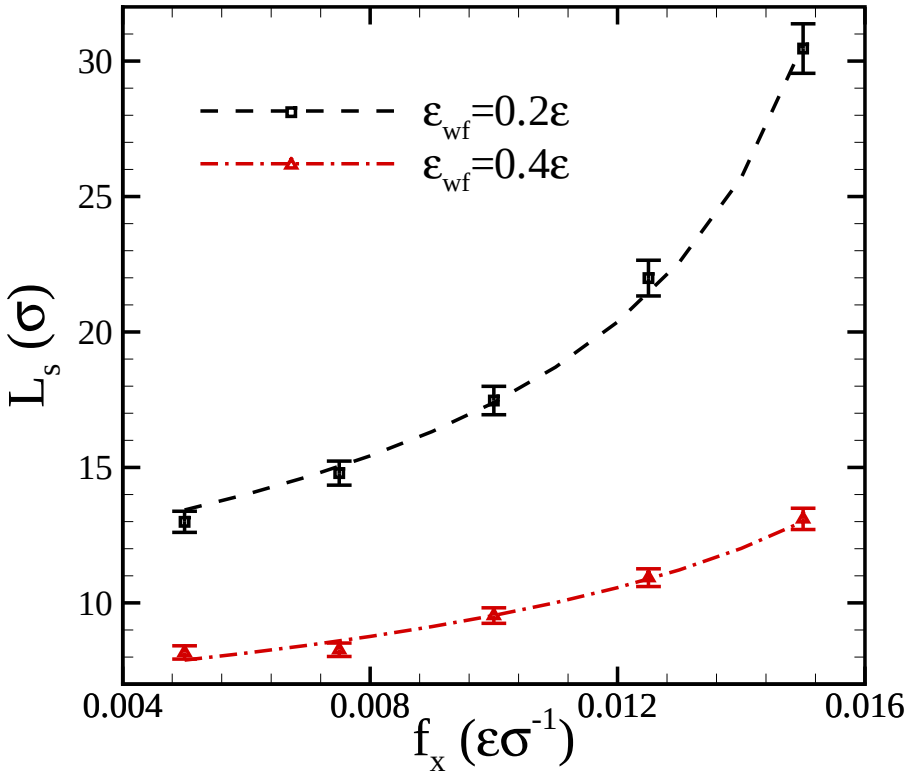


FIG. 2: Slip length variations with length $L_s$ as a function of the driving force $f_x$ for wall particles with stiffness $\kappa = 900\ \epsilon\sigma^{-2}$; the dashed curves are the best fitting to $L_s(f_x) = L_s^0\ (1 - f_x/f_c)^{-0.5}$.

Figure 3 shows an example of the slip length as a function of surface stiffness. In the performed molecular simulations the interaction parameters are $\epsilon_{wf} = 0.4\epsilon$, $\sigma_{wf} = 0.75\sigma$ and the external driving force is $f_x = 0.01\ \epsilon\sigma^{-1}$. In Fig. 3 the slip length has been scaled over the parameter $L_0$, which represents the slip length when a fixed lattice wall is employed. In this wall model the solid particles are immobilised in their lattice sites and, therefore, are not allowed to vibrate [7, 23]. Figure 3 shows that the slip varies along with the surface stiffness indicating its importance to the slip process. It is visible that for the less stiff surfaces, such as $\kappa = 100\ \epsilon\sigma^{-2}$ for the example of Fig. 3, the degree of slip is smaller compared to the one calculated when a fixed lattice wall is employed. Smaller values of $\kappa$ imply larger displacements of the wall particles resulting to an increased surface roughness. In this case the interactions between the wall's and fluid's particles are enhanced leading

to improved momentum transfer and consequently to less slippage. As $\kappa$ increases the wall's surface becomes effectively smoother and higher slip is produced. However, it can be observed in Fig. 3 that the slip length, instead of increasing monotonically with the wall's stiffness, it obtains a maximum value $L_{s,max}$ and then starts to decline. Although stiffer walls are employed the impact of bonding stiffness to the oscillation amplitude of the walls' particles is continuously decreasing. The amplitude, as already mentioned, is primarily dictated from walls' temperature and therefore $\kappa$ is no longer a dominant factor for the surface smoothness or roughness. In these cases, increasing the values of $\kappa$ alters the oscillation frequency towards higher values that contribute to a more efficient interfacial momentum transfer and consequently to a reduction in the slip length. This is justified for values of stiffness $\kappa$ that lead to oscillating periods $T_{oscill}$ higher than the mean molecular collision time ($\tau_{coll}$); for the current study this is valid for $\kappa < 2000\ \epsilon\sigma^{-2}$.

The relative growth and decay of the mean frequency and amplitude respectively, as a function of $\kappa$ are shown in Fig. 4. These variations are calculated as $(f_\kappa - f_{\kappa=100})/f_{\kappa=100}$ and $(d_{\kappa=100} - d_\kappa)/d_{\kappa=100}$, where $f$ corresponds to the mean oscillating frequency and $d$ to the mean vibrating amplitude of the wall particles. The values for $\kappa = 100\ \epsilon\sigma^{-2}$ are $f_{\kappa=100} = 1.672\ 1/\tau$, corresponding to a mean oscillation time $T_{oscill,\kappa=100} = 0.598\ \tau$, and $d_{\kappa=100} = 5.3 \cdot 10^{-4}\ \sigma$. Figure 4 shows that for higher stiffness values there is almost a linear increase for the frequency and concurrently the decay rate of the mean displacement approaches to zero.

Similar behaviour has been observed in all the performed simulations regardless the various wall-fluid interactions or shear rates employed. The results of the numerical experiments are summarised in Fig. 5. Here, the slip length has been scaled over the $L_{s,max}$, which represents its maximum value in a series of simulations with the same interaction parameters, driving force and variable $\kappa$. The stiffness has been scaled over the $\kappa_{max}$, which represents the value of $\kappa$ that maximises the slip. It is apparent that the parameters $L_{s,max}$ and $\kappa_{max}$ depend upon the various simulations conditions such as shear rate or surface attraction energy. Figure 5 shows that the effect of the wall's stiffness to the slip process can be well quantified by a master curve, which in our case is a fifth order polynomial

$$\frac{L_S}{L_{S,max}} = a + b \cdot \frac{\kappa}{\kappa_{max}} + \cdots + f \cdot \left(\frac{\kappa}{\kappa_{max}}\right)^5 \tag{6}$$

where $a = 0.01$,$b = 2.59$, $c = -1.68$, $d = -0.77$, $e = 1.16$ and $f = -0.32$. In addition, Fig.

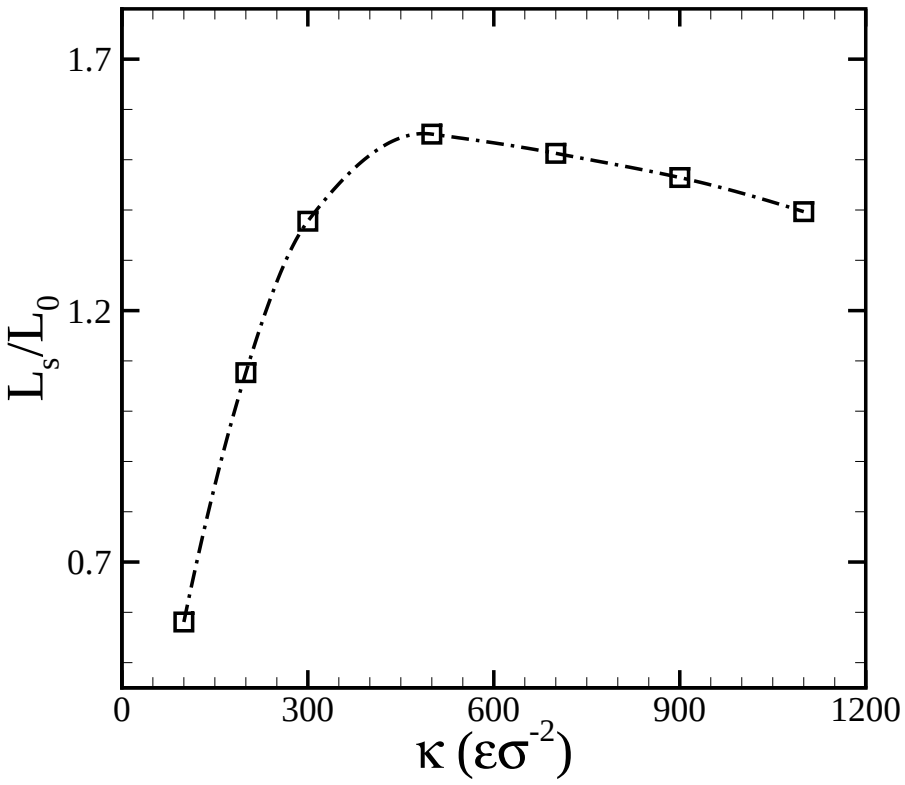


FIG. 3: Variation of the slip length as a function of surface stiffness for a flow with $f_x = 0.01\epsilon\sigma^{-1}$, $\epsilon_{wf} = 0.4\epsilon$.

5 suggests that the selection of the wall's stiffness during the molecular simulations should be made cautiously since it can lead to various slip scenarios. Potentially the master curve can be extended to accommodate the variation of $L_{s,max}$ and $\kappa_{max}$ as functions of other parameters that are important to the slip process, like for example the shear rate.

## IV. CONCLUDING OVERVIEW

In summary, this study has investigated the relationship between the wall stiffness and the slip produced. For the first time we show that the slip length variations as a function of surface stiffness can be approximated and well described through a master curve. Quantifying the dependence of $L_s$ on $\kappa$ provides a mechanism for obtaining a better insight in the slip phenomena and reducing the variability regarding the values of surface stiffness employed in molecular simulations. Generally, the stiffness factor influences not only the slip process

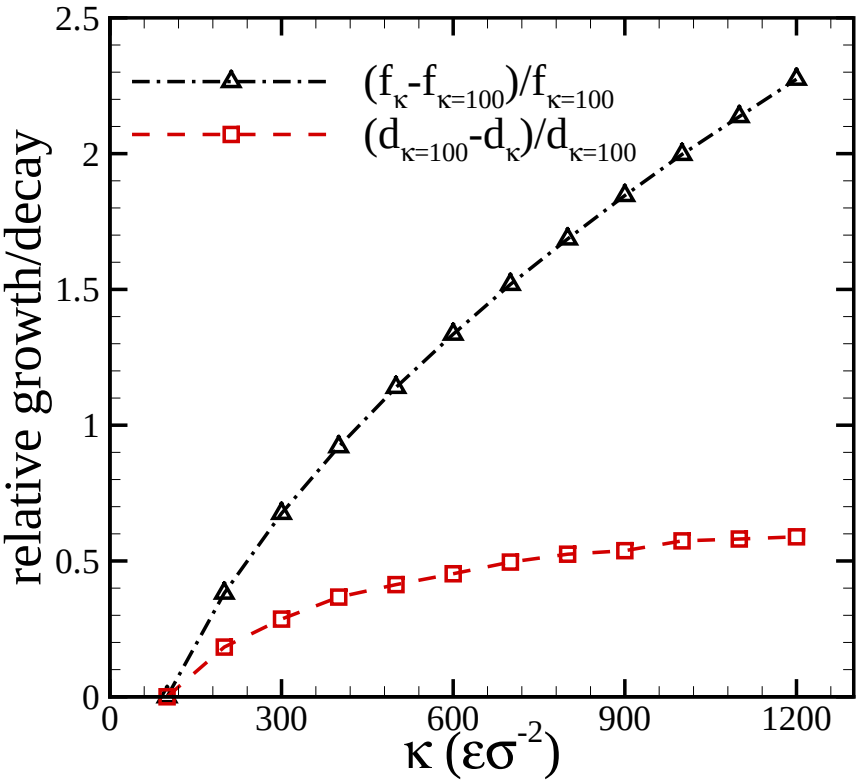


FIG. 4: Relative variations of the mean oscillation amplitude and frequency (with respect to mean amplitude and frequency for $\kappa = 100$) as a function of stiffness $\kappa$.

but also the thermal equilibrium at the solid liquid interface [23]. Further studies towards a better understanding of the stiffness effects on the slip and thermal transfer phenomena are also currently being pursued. Specifically, the combined effects of wall particles' mass with the surface stiffness are studied along with more realistic models for the thermal walls.

[1] C. Choi, K. Westin, and K. Breuer, Physics of Fluids **15**, 2897 (2003).

[2] D. C. Tretheway and C. D. Meinhart, Physics of Fluids **14**, L9 (2002).

[3] Y. Zhu and S. Granick, Phys. Rev. Lett. **88**, 1061021 (2002).

[4] M. Sbragaglia, R. Benzi, L. Biferale, S. Succi, and F. Toschi, Phys. Rev. Lett. **97**, 204503 (2006).

[5] N. V. Priezjev, A. A. Darhuber, and S. M. Troian, Phys. Rev. E **71**, 041608 (2005).

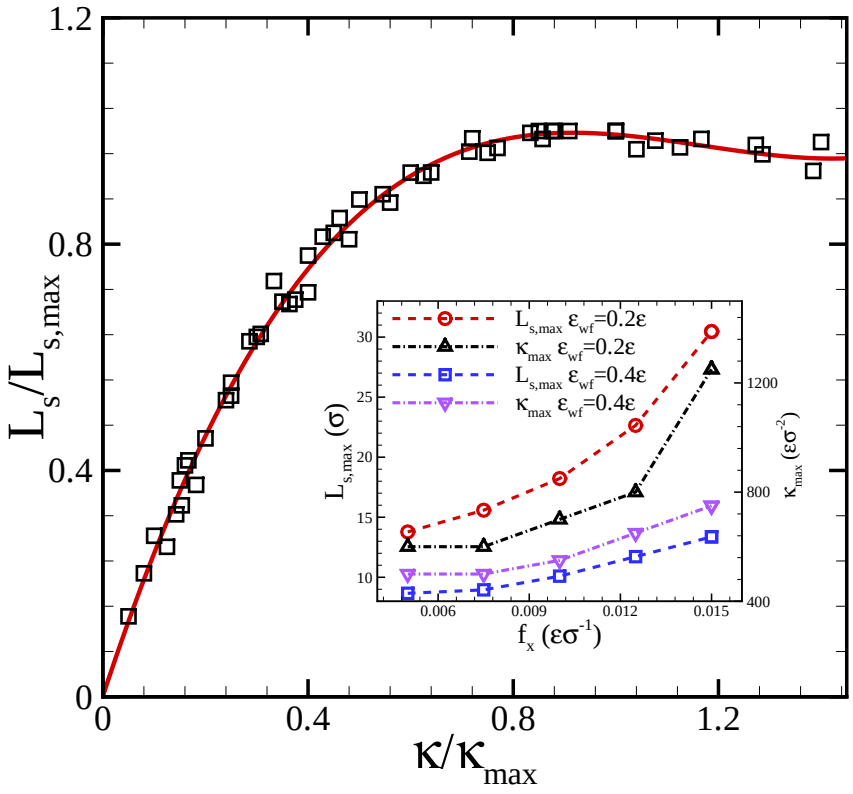


FIG. 5: Master curve describing the variation of the slip length as a function of wall stiffness. The inset shows how the values $L_{s,max}$ and $\kappa_{max}$ varies with the driving force $f_x$ for the different interaction parameters.


[6] C. Cottin-Bizonne, J. Barrat, L. Bocquet, and E. Charlaix, Nature Mater. **2**, 237 (2003).

[7] P. A. Thompson and S. M. Troian, Nature **389**, 360 (1997).

[8] J. Barrat and L. Bocquet, Phys. Rev. Lett. **82**, 4671 (1999).

[9] N. V. Priezjev, J. Chem. Phys. **127**, 144708 (2007).

[10] C. Cottin-Bizonne, C. Barentin, E. Charlaix, L. Bocquet, and J. Barrat, Eur. Phys. J. C **15**, 427 (2004).

[11] E. Bonaccurso, H.-J. Butt, and V. S. J. Craig, Phys. Rev. Lett. **90**, 144501 (2003).

[12] T. M. Galea and P. Attard, Langmuir **20**, 3477 (2004).

[13] N. V. Priezjev and S. M. Troian, J. Fluid Mech. **554**, 25 (2006).

[14] F. D. Sofos, T. E. Karakasidis, and A. Liakopoulos, Phys. Rev. E **79**, 026305 (2009).

[15] Y. Zhu and S. Granick, Phys. Rev. Lett. **87**, 961051 (2001).

[16] K. Binder, J. Horbach, W. Kob, P. Wolfgang, and V. Fathollah, J. Phys. Cond. **16**, S429 (2004).

[17] G. S. Grest and K. Kremer, Phys. Rev. A **33**, 3628 (1986).

[18] M. P. Allen and D. J. Tildesley, *Computer simulation of liquids* (Oxford University Press, Oxford, 1987).

[19] J. L. Barrat and J. P. Hansen, *Basic concepts for simple and complex liquids* (Oxford University Press, Oxford, 2003).

[20] A. Jabbarzadeh, J. D. Atkinson, and R. I. Tanner, J. Chem. Phys. **110**, 2612 (1999).

[21] M. Cieplak, J. Koplik, and J. R. Banavar, Phys. Rev. Lett. **86**, 803 (2001).

[22] K. Petersen, IEEE Tran. Elec. Dev. **25**, 1241 (1978).

[23] B. H. Kim, A. Beskok, and T. Cagin, Microfluidics and Nanofluidics **5**, 551 (2008).

[24] J. Koplik, J. R. Banavar, and J. F. Willemsen, Phys. Rev. A **1**, 781 (1989).

[25] P. A. Thompson and M. O. Robbins, Phys. Rev. A **41**, 6830 (1990).

[26] P. Yi, D. Poulikakos, J. Walther, and G. Yadigaroglu, International Journal of Heat and Mass Transfer **45**, 2087 (2002).

[27] R. Branam and M. Micci, Nanosc. Microsc. Thermoph. Eng. **13**, 1 (2009).